

Author Manuscript

Title: Catalytic Hydrogenolysis of the Pt-OPh Bond of a Molecular Pt(II) Complex using Silica Supported Pd, Rh and Pt Nanoparticles

Authors: Zhongwen Luo; Jiahan Xie; Nicholas Kaylor; Diane Dickie; Robert Davis; Thomas Brent Gunnoe

This is the author manuscript accepted for publication. It has not been through the copyediting, typesetting, pagination and proofreading process, which may lead to differences between this version and the Version of Record.

To be cited as: 10.1002/cctc.202200582

Link to VoR: <https://doi.org/10.1002/cctc.202200582>

Catalytic Hydrogenolysis of the Pt–OPh Bond of a Molecular Pt(II) Complex using Silica Supported Pd, Rh and Pt Nanoparticles

Zhongwen Luo^a, Jiahua Xie^b, Nicholas Kaylor^b, Diane A. Dickie^a, Hannah E. Ketcham^a, Robert J. Davis,^{*,b} and T. Brent Gunnoe^{*,a}

^a Department of Chemistry, University of Virginia, Charlottesville, VA 22904

^b Department of Chemical Engineering, University of Virginia, Charlottesville, VA 22904

E-mail: tbg7h@virginia.edu

Email: rjd4f@virginia.edu

Abstract

Silica-supported Pd, Rh and Pt metal nanoparticles catalyze the hydrogenolysis of the Pt–OPh bond of (^tbpy)Pt(OPh)Cl to release PhOH. Based on kinetic studies monitored by ¹H NMR spectroscopy, the reactivity trend is Pd > Rh > Pt. Kinetic studies with Pd/SiO₂ are consistent with a first-order dependence on the catalyst and the molecular Pt(II) complex (^tbpy)Pt(OPh)Cl. Using TEM-EDS mapping and ICP-OES measurements of a recovered Pd catalyst, after 1 hour of hydrogenolysis of (^tbpy)Pt(OPh)Cl, approximately 10-16% Pt deposition (relative to Pd mol%) on the Pd/SiO₂ surface was quantified.

Author Manuscript

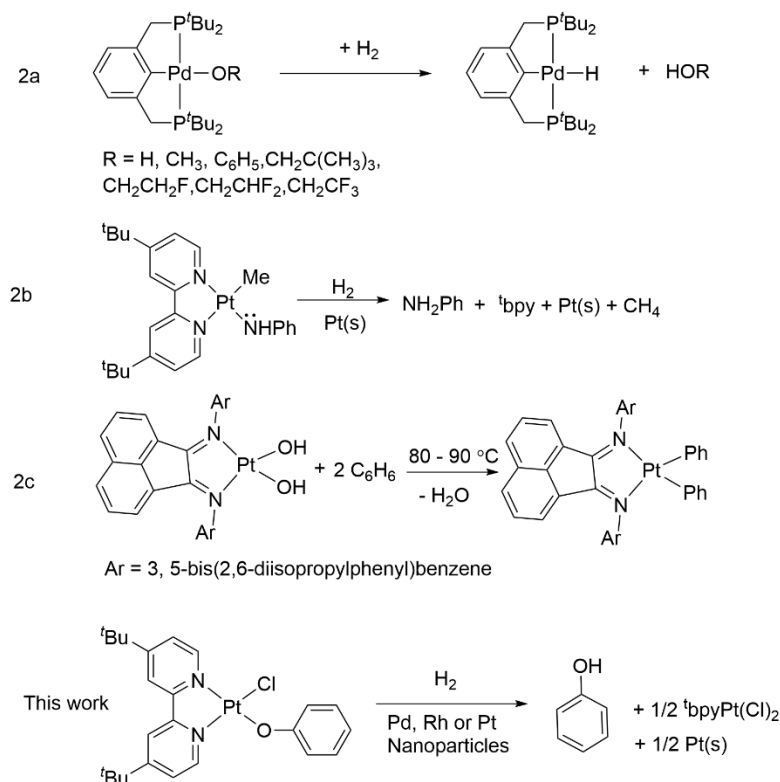
Introduction

The use of dihydrogen in chemical synthesis generally involves two broad reaction classes: hydrogenation and hydrogenolysis reactions. Hydrogenation reactions of olefins, aldehydes and ketones play an important role in the synthesis of high-value chemicals, intermediates, and active pharmaceutical ingredients.^{[1],[2]} Examples of catalytic hydrogenolysis include alkane hydrogenolysis to produce lighter alkanes^[3] and hydrogenolysis of C–O bonds of biomass derived platform molecules.^[4] Hydrogenolysis reactions are of particular interest for the conversion of molecules from biomass to more valuable products, which commonly involves a reaction process involving hydrogenation followed by dehydration^[5] and hydrodeoxygenation of biomass derived compounds.^[5c, 6]

Net hydrogenolysis of ether and alcohol groups is a key transformation.^[7] For transition metal catalyzed deoxygenation, the formation of metal alkoxide, aryloxy and/or hydroxide intermediates is sometimes invoked in reaction pathways for deoxygenation processes,^[8] and, hence, understanding reactions of M–OR (R = alkyl, aryl or H) groups with dihydrogen, particularly to release ROH, is of interest.^[8b, 8c, 8e, 9] For example, Goldberg and co-workers demonstrated that hydrogenolysis of palladium(II) hydroxide, phenoxide and alkoxide complexes release corresponding HOR (R = H, CH₃, C₆H₅ and CH₂(CH₃)₃) (Scheme 1a).^[8b, 8c] Similarly, hydrogenolysis of platinum(II) hydroxide and amido complexes was observed by the Gunnoe group (Scheme 1b).^[8d, 8f, 10] In studies of net hydrogenolysis of a Pt(II) anilido complex, an induction period was observed,^[8d, 8e, 10] which was attributed to the *in situ* formation of elemental Pt that served as a catalyst for the hydrogenolysis. In addition, Piers and coworkers observed that *in situ*

formation of reduced Pt nanoparticles can serve as the catalyst promoting the addition of benzene C–H bonds across Pt(II)-hydroxide bonds (Scheme 1c).^[8e]

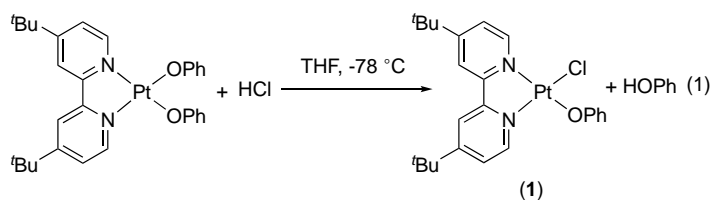
In this study, we examined the use of silica-supported Pd, Rh, and Pt nanoparticles as catalysts for the hydrogenolysis of a M–OR bond. Specifically, we investigated catalytic performance towards hydrogenolysis of the Pt–OPh bond of (t₁bpy)Pt(OPh)Cl (**1**) to form PhOH (Scheme 1d). We note that such a reaction could be considered a hydrogenolysis, since the observed products, including free PhOH, are the result of cleavage of the Pt–OPh bond, but, also, the initial kinetic product likely has phenol coordinated to Pt(II) and, hence, retention of the Pt–O bond, which makes a case for the reaction to be considered as a hydrogenation process. Herein, we refer to the overall process with phenol production (i.e., hydrogenolysis).



Scheme 1. Examples of hydrogenolysis of Pd–OR, Pt–NHPh and Pt–OR bonds.

Results and Discussion

Synthesis of molecular Pt(II) phenoxide complex. The complex (^tbpy)Pt(OPh)Cl (**1**) (^tbpy= 4,4'-di-tert-butyl-2,2'-bipyridine) was synthesized by reacting (^tbpy)Pt(OPh)₂ with one equivalent HCl at -78 °C, and ~70% isolated yield was obtained (eq 1).



Complex **1** was characterized by ¹H and ¹³C NMR spectroscopy, elemental analysis and single crystal X-ray diffraction. A single crystal of **1** was grown by slow evaporation of a pentane/acetone solution (Figure 1). As expected, the geometry around the Pt center is square planar. The Pt–O bond distance of complex **1** is 1.988(10) Å, which is similar to the Pt–O distances of (^tbpy)Pt(OPh)₂ (2.001(4) Å and 2.014(4) Å).^[8d] The Pt–O–C bond angle is 124.3(9)°.

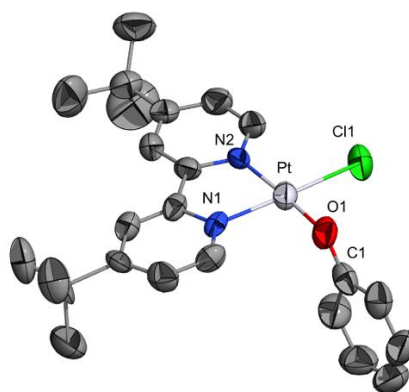


Figure 1. ORTEP of (^tbpy)Pt(OPh)Cl (**1**) (30% probability). Hydrogen atoms have been omitted for clarity. Selected bond lengths (Å) and angles (°): Pt–N(1) = 2.042(8), Pt–N(2) = 1.997(11), Pt–O(1) = 1.988(10), Pt–Cl(1) = 2.292(3), C(1)–O(1)–Pt = 124.3(9), Cl(1)–Pt–O(1) = 90.6(3), Cl(1)–Pt–N(2) = 95.0(3), O(1)–Pt–N(1) = 93.1(4), N(1)–Pt–N(2) = 81.3(4). An acetone co-solvent molecule and protons are removed for clarity.

Synthesis of silica-supported Pd, Rh and Pt nanoparticles. Uniform noble metal catalysts on silica support (Pd/SiO₂, Rh/SiO₂ and Pt/SiO₂) were synthesized via an ion exchange method based on literature procedures.^[11] The supported nanoparticle materials were characterized by ICP-OES and TEM (see Supporting Information).^[11b-d, 12] Analyses by ICP-OES indicated the following metal compositions: 5.0 wt% Pd (Pd/SiO₂), 1.0 wt% Pt (Pt/SiO₂) and 3.6 wt% Rh (Rh/SiO₂).^[11b-d, 12] Typical HAADF–STEM images of Pd/SiO₂ and Rh/SiO₂ are shown in Figure 2. The particle size distribution analysis of the synthesized Pd/SiO₂ material indicated that the Pd nanoparticles were approximately 1.1(4) nm in diameter, and the nanoparticles are well dispersed on the silica support. Analysis by H₂ chemisorption, assuming a H/Pd_{surface} ratio of unity, indicated the fraction of Pd atoms exposed to the surface was 80%, which is consistent with the nanometer particle size evaluated by electron microscopy. For the analyses of catalyst performance, surface Pd atoms are assumed to be the catalytically active sites. The same characterization techniques were used for Pt/SiO₂^[11c] and Rh/SiO₂^[11d] materials. Dihydrogen chemisorption of the synthesized Rh/SiO₂ material indicated a fraction of Rh exposed to be ~70% and the average Rh metal particle size measured by TEM was found to be 2.2(5) nm.^[11d] Using H₂ chemisorption, the fraction of Pt exposed on Pt/SiO₂ was determined to be 40%, suggesting that the Pt particles on Pt/SiO₂ are approximately 3.0 nm.^[13]

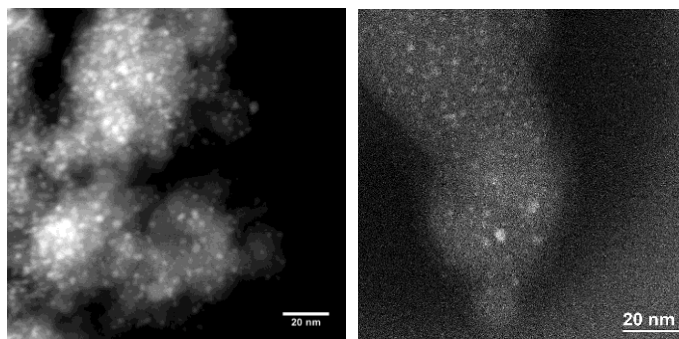
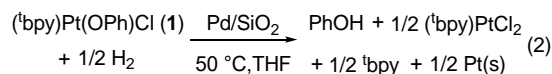


Figure 2. A HAADF-STEM image of synthesized SiO₂ supported Pd nanoparticles (Pd/SiO₂, left) and Rh nanoparticles (Rh/SiO₂, right).

Catalytic hydrogenolysis of (^tbpy)Pt(OPh)Cl (1). The reaction of complex **1** with 20 psig H₂ in THF at 50 °C in the presence of Pd/SiO₂ as catalyst resulted in the net hydrogenolysis of the Pt–OPh bond of complex **1** to produce phenol in ~83% yield by ¹H NMR spectroscopy, (^tbpy)PtCl₂ in ~36% yield, free ^tbpy in ~40% yield and Pt(s) (eq 2). The reaction is complete after approximately 6 hours. A control reaction between **1** with H₂ (20 psig) in the absence of the Pd/SiO₂ produced phenol at a greatly reduced rate (< 10% conversion after 8 h compared to almost 80% conversion after 6 h when Pd/SiO₂ was used). In a control experiment, complex **1** was combined with silica and heated to 50 °C for 3 hours with no observation of phenol. These observations are consistent with the Pd/SiO₂ catalyzing the hydrogenolysis of **1**.



We used ¹H NMR spectroscopy to monitor the kinetics of hydrogenolysis of complex **1** (Figure S3). In a typical experiment, the resonance at 6.3 ppm (assigned as the para H of the phenyl group) was used to quantify the conversion of complex **1**. Resonances due to the formation of PhOH (6.6, 7.1 and 8.1 ppm), free ^tbpy (7.3, 8.5 and 8.6 ppm) and (^tbpy)PtCl₂ (7.6, 8.2 and 9.4 ppm) were used to quantify the formation of products. A

typical concentration profile of PhOH (red) and (^tbpy)Pt(OPh)Cl (**1**) (blue) is shown in Figure 3.

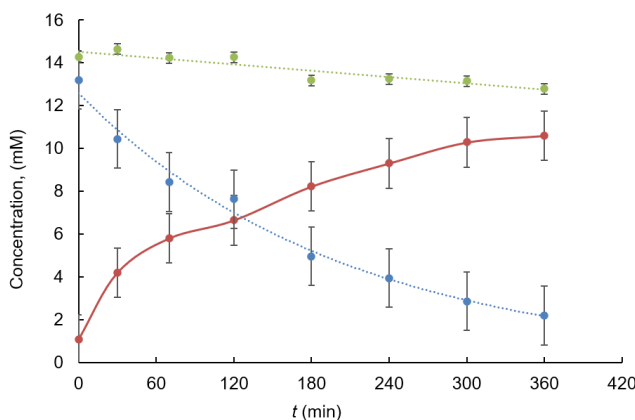


Figure 3. Concentrations of reactants and products from Pd/SiO₂ catalyzed hydrogenolysis of (^tbpy)Pt(OPh)Cl (**1**): Sum of the concentrations of complex **1** and PhOH (green), concentration of PhOH (red), and concentration of (^tbpy)PtCl(OPh) (blue). Reaction conditions: (^tbpy)Pt(OPh)Cl (13.2 mmol/L), 20 psig H₂ (~7-11 mmol/L in solution), Pd/SiO₂ (5 wt%, 1.1 × 10⁻⁶ mol Pd_{surf}), 50 °C, THF-*d*₈, internal standard hexamethyldisilane (2.33 mmol/L).

For the hydrogenolysis of **1** at 50 °C, a first-order dependence on complex **1** was determined for the Pd nanoparticle catalyzed hydrogenolysis (Figure 4), which contrasts previously reported hydrogenolysis of the Pt–NHP bond of (^tbpy)Pt(NHP)(CH₃), which exhibited a zero-order dependence on (^tbpy)Pt(NHP)(CH₃).¹⁶ The previously reported zero-order dependence on the (^tbpy)Pt(NHP)(CH₃) complex is explained by an initial induction period during which decomposition of (^tbpy)Pt(NHP)(CH₃) to form heterogeneous Pt nanoparticles occurs, which is followed by catalytic hydrogenolysis of the Pt–NHP moiety of (^tbpy)Pt(NHP)(CH₃) in a process that is first-order in H₂. For our current kinetic studies, H₂ in solution is replenished from the gas phase as the reaction progresses (Figure S4), and, thus, our kinetic studies are under conditions that are effectively pseudo first-order in **1**.

The rate of hydrogenolysis of **1** using Pd/SiO₂ as catalyst was found to be proportional to the number of surface Pd atoms in the reactor. Monitoring the catalytic plot of k_{obs} versus relative amount of surface Pd (Figure 5, the x-axis is the ratio of surface palladium sites and complex **1**). The k_{obs} was determined from the slope of the first-order kinetic plot of $\ln[\text{PtOPh}]$ vs. time. We found that k_{obs} increased by approximately 5-fold by increasing the amount of Pd catalyst by 5 times. This linear dependence on the amount of Pd nanoparticles indicates that the surface Pd atoms are likely responsible for the accelerated hydrogenolysis rate of complex **1** to release PhOH.

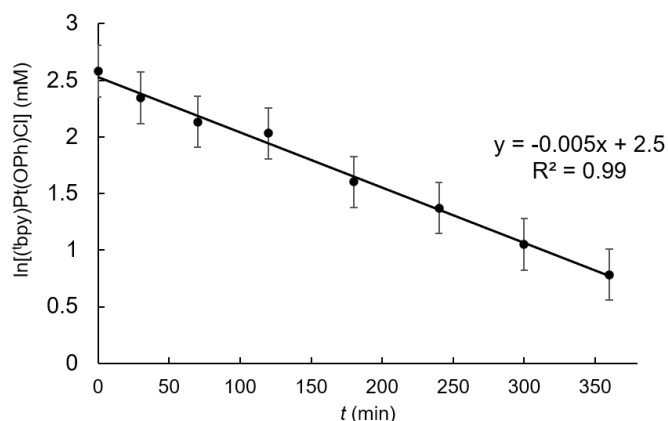


Figure 4. Plot of $\ln[(\text{bpy})\text{Pt}(\text{OPh})\text{Cl}]$ versus time is consistent with a reaction that is first-order in complex **1**. Reaction conditions: $(\text{bpy})\text{Pt}(\text{OPh})\text{Cl}$ (13.2 mmol/L), 20 psig H₂ (~7-11 mmol/L in solution), Pd/SiO₂ (5 wt%, 1.1×10^{-6} mol Pd_{surf}), 50 °C, THF-*d*₈, internal standard hexamethyldisilane (2.33 mmol/L).

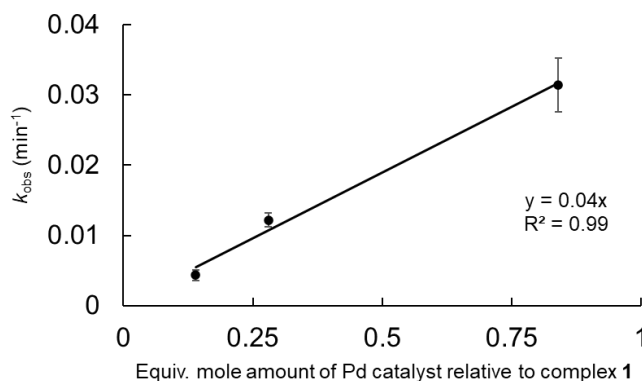


Figure 5. A plot of k_{obs} versus amount of Pd/SiO₂ loading. Reaction conditions: (^tbpy)Pt(OPh)Cl (**1**) (13.2 mmol/L), 20 psig H₂ (~7–11 mmol/L in solution), Pd/SiO₂ (5 wt%, 1.1 x 10⁻⁶ mol, 2 x 10⁻⁶ mol, and 6 x 10⁻⁶ mol Pd_{surf}), 50 °C, THF-*d*₈; hexamethyldisilane (2.33 mmol/L).

During the hydrogenolysis of **1** in the presence of Pd/SiO₂, evidence of deposition of elemental Pt on the Pd surface was obtained. After 1 hour of hydrogenolysis of **1** at 50 °C in the presence of 20 psig H₂, TEM-EDS mapping of Pt, Pd and Si of the recovered solid revealed approximately 16 mol% Pt (relative to Pd) on the Pd/SiO₂ surface (Figure 6). Inductively coupled plasma optical emission spectroscopy (ICP-OES) measurements further confirmed and quantified the deposition of Pt on Pd/SiO₂ with approximately 10 mol% (relative to Pd) atomic Pt deposited. Particle size analysis of the Pd nanoparticles following 1 hour of hydrogenolysis of complex **1** revealed that the average size of the metal nanoparticles increased from 1.1(4) nm to approximately 2.0(5) nm in diameter (Figure 7), which is consistent with the observation of Pt deposition.

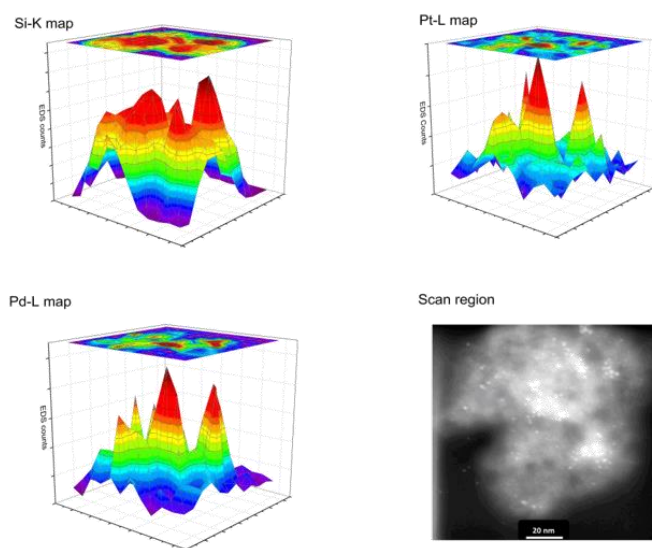


Figure 6. TEM-EDS mapping of selective areas of supported Pd nanoparticles (on silica) after 1 h of reaction. Reaction conditions: (^tbpy)Pt(OPh)Cl (**1**) (13.2 mmol/L), 20 psig H₂ (~7–11 mmol/L in solution), Pd/SiO₂ (5 wt%, 3 mg, 1.1 x 10⁻⁶ mol Pd_{surf}), 50 °C, THF-*d*₈, internal standard hexamethyldisilane (2.33 mmol/L).

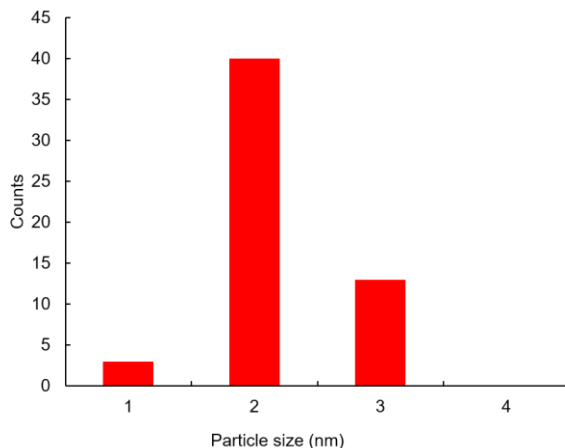


Figure 7. The particle size distribution of recovered Pd nanoparticles (on silica) measured by TEM analysis after 1 h of hydrogenolysis of (*t*-bpy)Pt(OPh)Cl (**1**). Reaction conditions: (*t*-bpy)Pt(OPh)Cl (**1**) (13.2 mmol/L), 20 psig H₂ (~7-11 mmol/L in solution), Pd/SiO₂ (5 wt%, 3 mg, 1.1 × 10⁻⁶ mol Pd_{surf}), 50 °C, THF-*d*₈, internal standard hexamethyldisilane (2.33 mmol/L).

In order to evaluate relative efficacy of other metals in the hydrogenolysis of complex **1**, we prepared nanoparticles of Rh and Pt on silica with 3.6 wt% Rh/SiO₂ and 1.0 wt% Pt/SiO₂ and tested their catalytic efficacy. We compared the catalytic hydrogenolysis of **1** using the Rh/SiO₂ and Pt/SiO₂ materials to the Pd/SiO₂ material. At a relatively low conversion of complex **1**, Table 1 shows a comparison of TOFs for the Pd, Rh, and Pt nanoparticles {TOF = (mole of complex **1** reacted)/(mole of surface atoms)/t(s), note surface atoms are the fraction of nanoparticles estimated by hydrogen chemisorption}. The TOFs were calculated from the initial rates of reaction evaluated at relatively low conversion: a) for the Pd/SiO₂ reaction, the TOF was determined after 1 hour of reaction (~35% conversion), b) for the Rh/SiO₂ reaction, the TOF was determined after 4 hours of reaction (~25% conversion), and c) for the Pt/SiO₂ reaction, the TOF was determined after 4 hours of reaction (~5% conversion). With equivalent amounts of catalyst loading, the rate of hydrogenolysis of **1** follows the trend: Pd > Rh > Pt. Relative to Pt, the Pd nanoparticles gave a TOF that is approximately 5.2 times faster, while the Rh nanoparticles TOF value is 1.4 times larger than Pt. Although the liquid hydrogenolysis

rate is much slower compared with that of C=C hydrogenation, the relative rate trend mediated by different nanoparticle is consistent with previously reported results for the liquid phase olefin hydrogenation with noble metal catalysts, which is Pd > Rh > Pt.^[14] Importantly, the differences in rate of dihydrogen addition across the Pt–OPh bond and C=C bonds based on metal identity are more pronounced for the former. Although we cannot, at this time, rationalize the trends based on metal identity for dihydrogen addition to the Pt–OPh bond, it is clear that this reaction, which likely involves a net heterolytic addition of a proton to the phenoxide ligand and a hydride to Pt, is much different in nature than the dihydrogen addition across a C=C bond.

Table 1. Liquid phase TOFs for nanoparticles catalyzed Pt–OPh hydrogenolysis and C=C hydrogenation

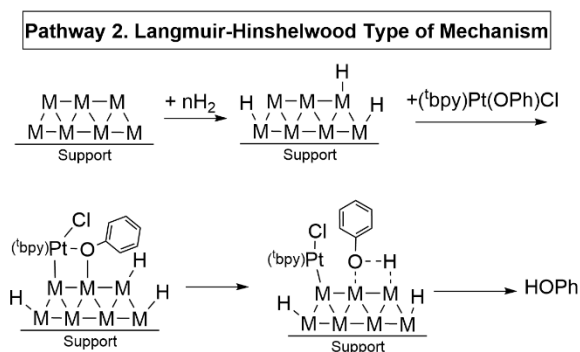
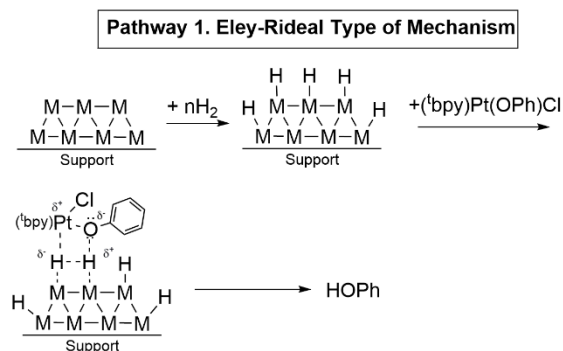
Pt–OPh ^a , s ⁻¹	C=C ^[14] , s ⁻¹
2.5(6)×10 ⁻⁴ (Pd/SiO ₂)	1.35–1.72 (supported Pd) ^b
6.9(4)×10 ⁻⁵ (Rh/SiO ₂)	1.16–1.36 (supported Rh)
4.9(4)×10 ⁻⁵ (Pt/SiO ₂)	0.55–0.66 (supported Pt)

^a TOF = (mole of complex **1** reacted)/(mole of surface atoms)/t(s). Reaction conditions: 10 mM complex **1** in 0.5 mL THF-*d*₆, ~1.1 × 10⁻⁶ mol surface Pd, Pt and Rh atoms, 20 psig hydrogen, 50 °C and 2 mM hexamethyldisilane as an internal standard. ^b A typical reaction condition for liquid phase cyclohexene hydrogenation: solvent cyclohexane, 25 °C and 14.7 psi H₂.

Despite Pt deposition on the Pd nanoparticles, the observed rates of reaction appear to retain a first-order dependence on complex **1**. Given that Pt nanoparticles were not as active as Pd nanoparticles for the hydrogenolysis of **1** (*vide supra*), deposition of Pt onto the Pd nanoparticles is expected to potentially decrease the rate of hydrogenolysis by reducing access to Pd active sites. It is possible that in the presence of H₂, Pd atoms migrate to the surface of the nanoparticles despite the deposition of Pt atoms.^[15]

It is difficult to elucidate the operative pathway for phenol formation in the gas-solid-liquid interface because there is no straightforward technique to observe the interaction between a homogeneous molecular complex and a heterogeneous material. Also, *in situ*

^1H NMR spectroscopy did not reveal molecular Pt intermediates. Two possible mechanisms, among many possibilities, for Pt–OR bond hydrogenolysis are shown in Schemes 3 and 4. In pathway 1, H_2 is activated heterolytically^[16] and transferred across the Pt–OPh bond as H^+/H^- in an Eley–Rideal type mechanism without the direct interaction of the Pt complex with the nanoparticle surface.^[17] Phenol is formed upon proton transfer from the metal surface to phenoxide ligand (Scheme 2). In contrast, pathway 2 (Scheme 3) involves the initial cleavage of both the H–H and Pt–OPh bonds to generate surface-bound phenoxide and hydrogen atoms via a Langmuir-Hinshelwood type of mechanism.^[18] In this pathway, the $(^t\text{bpy})\text{Pt}$ –OPh species would be initially adsorbed to the Pd surface followed by Pt–OPh bond cleavage, and then surface OPh and H atom combination would release HOPh.



We used Raman spectroscopy in an effort to observe intermediates of potential relevance to the catalytic process. Pd/SiO₂ was reacted with complex **1** in THF at 50 °C in the presence of 20 psig of H₂ for 1 h and recovered the solid Pd/SiO₂. Raman spectroscopy of the recovered Pd/SiO₂ indicated that a (^tbpy)Pt(OPh)Cl species might be absorbed on the nanoparticle surface (Figure 8). This hypothesis is supported by the observation of features consistent with a Pt–O vibration (~573 cm⁻¹),^[19] a C–O bending mode (~505 cm⁻¹), and a C–O stretching mode (~1240 cm⁻¹) in the Raman spectrum. Further evidence for the formation of Pd absorbed (^tbpy)Pt(OPh)Cl was observed when the recovered Pd/SiO₂ was treated with 20 psig H₂ in THF at 50 °C for ~2 h, resulting in the release of free ^tbpy as observed by ¹H NMR spectroscopy (Figure S7). Using Raman and ¹H NMR spectroscopies, we hypothesize that the formation of surface bound molecular Pt species could occur during the catalysis. Whether such species are responsible for the catalytic activity is difficult to discern.

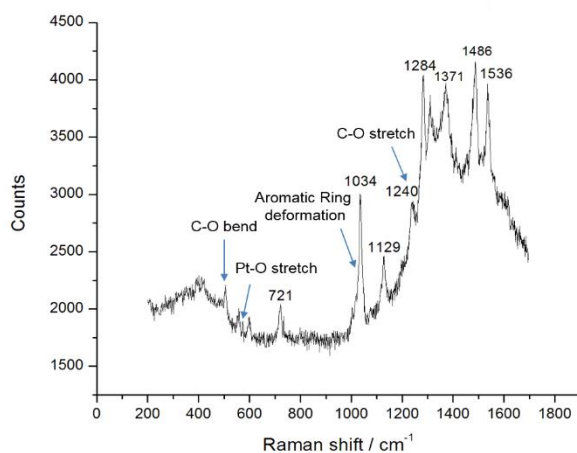


Figure 8. Raman spectrum of recovered Pd/SiO₂ material after hydrogenolysis of (^tbpy)Pt(OPh)Cl (**1**) for 1 h. Reaction conditions: (^tbpy)Pt(OPh)Cl (13.2 mmol/L), 20 psig H₂ (~7-11 mmol/L in solution), Pd/SiO₂ (5 wt%, 1.1 × 10⁻⁶ mol Pd_{surf}), T = 50 °C, THF-*d*₈, internal standard hexamethyldisilane (2.33 mmol/L).

Summary and Conclusions

Using (t₁bpy)Pt(OPh)Cl (**1**) as a probe molecule, it has been demonstrated that silica-supported Pd, Pt and Rh nanoparticles catalyze the hydrogenolysis of Pt–OPh bonds to release HOPh. Using ¹H NMR spectroscopy to monitor concentration changes in solution for the Pd/SiO₂ catalyzed reaction, a process that is first-order in complex **1** has been confirmed. *Ex situ* characterization of recovered Pd/SiO₂ using ¹H NMR and Raman spectroscopies revealed the possibility of adsorption of molecular Pt complexes on the Pd/SiO₂ surface, but current data are far from definitive, and a mechanistic proposal cannot be made. For the noble metal mediated hydrogenolysis of (t₁bpy)Pt(OPh)Cl complex and C=C bonds, they follow the reactivity trend: Pd > Rh > Pt. These results demonstrate the ability of heterogeneous materials to catalyze hydrogenation and/or hydrogenolysis reactions, which could have utility in its own right and is also relevant to possible decomposition of homogeneous molecular complexes into heterogeneous products that can serve as catalysts for various reactions.

Experimental Methods

General Methods. The glovebox purity was maintained by periodic dinitrogen purges and was monitored by a dioxygen analyzer (O₂ < 15 ppm for all reactions). THF-*d*₈ was distilled over sodium/benzophenone and was stored over 4Å molecular sieves. ¹H NMR and ¹³C NMR spectra were acquired using a 600 MHz (¹H NMR) and 201.2 MHz (¹³C NMR) and referenced using residual proton signals or the ¹³C resonance of the deuterated solvent. Medium-walled high-pressure glass NMR tubes with a PV-ANV Teflon valve (maximum pressure rating 150 psig) were purchased from Wilmad-Lab glass

and used for all 20 psig H₂ experiments. The NMR tubes were charged with H₂ using a stainless steel gas pressure line (maximum pressure rating 3000 psig) connected directly to the gas cylinder. Although the pressures were maintained well below the limits of the NMR tubes, all reactions were kept behind a blast shield. The complexes (t^hbpy)PtCl₂ and (t^hbpy)Pt(OPh)₂ were synthesized based on literature procedures.^[8f] Noble metal on silica catalysts were prepared by the ion exchange method.^[11b, 11d, 13] Compound 1 was deposited to CCDC depository with the deposition number of 2169989.

Synthesis of (t^hbpy)Pt(OPh)Cl (1). HCl (138 μl, 1M in diethyl ether) was added to 90 mg (0.138 mmol) of (t^hbpy)Pt(OPh)₂ dissolved in acetone (5 mL) and THF (30 mL). The reaction mixture was kept at -78 °C in a dry ice acetone bath for 30 minutes. Then, the dry ice bath was removed and the solution was allowed to slowly warm to room temperature. Upon addition of HCl, the color of the solution changed from orange to yellow. After 4 hours, the reaction mixture was condensed to approximately 1 mL under reduced pressure, and excess hexane was added to form a yellow precipitate. The precipitate was collected by vacuum filtration and washed with hexane (3 x ~20 mL) and diethyl ether (2 x 10 mL). The final product was obtained in approximately 70% yield, (~61 mg). ¹H NMR (600 MHz, acetone-*d*₆, ppm, Figure S1), 1.47 (s, 9H, t^hBu), 1.44 (s, 9H, t^hBu), 6.92 (t, ³J_{HH} = 9 Hz, 2H, *m*-OPh), 6.40 (t, ³J_{HH} = 7 Hz, 1H, *p*-OPh), δ = 7.14 (d, ³J_{HH} = 9 Hz, 2H, *o*-OPh), 7.83 (dd, ³J_{HH} = 6 Hz, ⁴J_{HH} = 2 Hz, 1H, t^hbpy), 7.81 (dd, ³J_{HH} = 6 Hz, ⁴J_{HH} = 2 Hz, 1H, t^hbpy), 8.57 (d, ⁴J_{HH} = 2 Hz, 1H, t^hbpy), 8.55 (d, ⁴J_{HH} = 2 Hz, 1H, t^hbpy), 8.85 (d, ³J_{HH} = 6 Hz, 1H, t^hbpy), 9.50 (d, 1H, 6 Hz, t^hbpy). ¹³C{¹H} NMR (200 MHz, acetone-*d*₆, ppm, Figure S2), δ = 29.4, (C(CH₃)₃), 29.4, (C(CH₃)₃), 35.8 (C(CH₃)₃), 35.9 (C(CH₃)₃), 114.3 (phenoxide, *p*-C), 119.4 (phenoxide, *o*-C), 120.9 (t^hbpy, *m*-C), 121 (t^hbpy, *m*-C), 124.3 (t^hbpy,

m-C), 124.2 (^tbpy, m-C), 127.9 (phenoxide, m-C), 146.6 (^tbpy, o-C), 150.1 (^tbpy, m-C), 156.5 (^tbpy, o-C), 157.5 (^tbpy, o-C), 164.3 (^tbpy, p-C), 164.4 (phenoxide, O-C), 168.6 (^tbpy, p-C). Anal. Calcd. for C₂₄H₂₉N₂ClOPt: C, 46.69; H, 4.94; N, 4.73 Found: C, 48.72; H, 4.92; N, 4.76. Single crystals suitable for X-ray diffraction analysis were obtained from a bilayer diffusion method, in which an acetone solution was layered with pentane at -1 °C. The crystal data and structure refinement for (^tbpy)Pt(OPh)Cl is shown in Table S1.

Synthesis of Silica-supported Noble Metal Nanoparticles. The 3.6 wt% silica-supported Rh nanoparticles (Rh/SiO₂) were prepared via an ion exchange method^[11a, 11b] of the Rh precursor using Davisil 636 silica (Sigma-Aldrich) as support. RhCl₃•3H₂O (0.250 g, 99%) was dissolved in a solution of aqueous ammonia (14.8 M, 28%-30% of NH₃ in water), which was prepared by dissolving 5.5 mL ammonium hydroxide in 282 mL distilled deionized water. The RhCl₃ solution was added dropwise over 10 min to 4.75 g of acid-washed Davisil 636 silica in 114 mL of distilled deionized water at 70 °C. The mixture was stirred for 60 min at 70 °C and then allowed to cool to room temperature. The slurry was filtered and collected. The filtrate was washed with water and vacuum dried overnight. After calcination in flowing air (medical grade) at 400 °C for 2 h, the sample was reduced in flowing dihydrogen (99.999%) at 250 °C for 2 h. After reduction, the system was evacuated and cooled to 30 °C for analysis. At 30 °C, the stoichiometric ratio of H to surface Rh is assumed to be 1:1. For the Pd catalyst, after reduction, the system was evacuated and cooled to 100 °C for analysis. The number of available metal sites was determined by extrapolating the high pressure, linear portion of the isotherm to zero pressure. At 100 °C, the stoichiometric ratio of H to surface Pd is 1:1. Using dihydrogen chemisorption on a Micromeritics ASAP 2020 adsorption system,^[11b] the

number of available metal sites was determined by extrapolating the linear portion of the isotherm to zero pressure with the assumption of no dihydrogen uptake on the support. Similarly, 5 wt% Pd/SiO₂ and 1 wt% Pt/SiO₂ were synthesized and characterized, as reported in the literature.^[11b, 11c]

Transmission Electron Microscopy (TEM). Samples analyzed by transmission electron microscopy (TEM) were prepared by dispersing the powders in cyclohexane or hexanes (99.5%, anhydrous, Sigma-Aldrich) and sonicating for 1 minute before mounting on Cu-supported holey carbon grids. The catalyst samples were imaged using an FEI Titan 80-300 operating at 300kV. The Pd/SiO₂ and Rh/SiO₂ samples were characterized in high angle annular dark field (HAADF) and scanning mode of TEM for single-nanoparticle composition analyses.

Kinetic Measurements. The reaction of (^tbpy)Pt(OPh)Cl (**1**) with H₂ in the presence of nanoparticles (Pd, Rh, and Pt on silica) was monitored by ¹H NMR spectroscopy using a 10 s relaxation time delay. To ensure reproducibility, each kinetic experiment was performed at least in triplicate. A representative procedure is given below. A medium-walled glass high-pressure NMR tube with a Teflon valve was charged with 0.5 mL of THF-*d*₈, (^tbpy)Pt(OPh)Cl (**1**) (0.0066 mmol, 0.0132 M), 3 mg of Pd on SiO₂ (5% wt. Pd loading, 1.1 x 10⁻⁶ mol Pd_{surf}), and hexamethyldisilane (0.002 M, as internal standard). An initial ¹H NMR spectrum was acquired. Then, the tube was charged with H₂ (~ 20 psig). The reaction mixture was monitored by ¹H NMR spectroscopy every hour until approximately 90% conversion to free HOPh, (^tbpy)PtCl₂ and ^tbpy was observed. The rate of the reaction was determined by monitoring the disappearance of ^tbpyPt(OPh)Cl (**1**) using the chemical shift at 6.31 ppm for reference. Note: the *k*_{obs} is extracted from the

slope of the first order kinetic plot of $\ln[\text{PtOPh}]$ versus different amount of Pd loading, (Figure S6). 0.14 Pd means that the molar ratio of surface Pd atoms in Pd/SiO₂ relative to complex **1** is 0.14. TOF calculation for Pd/SiO₂ is based on ~38% conversion of complex **1** while the TOFs calculation for Rh/SiO₂ and Pt/SiO₂ is estimated slightly below 20% conversion of the substrate.

Raman Spectroscopy. Sample was analyzed using a Renishaw InVia™ Confocal Raman Spectrometer. Raman spectra ranging from 100 to 2500 cm⁻¹ were recorded with a 785 nm laser operating at 7.6 mW and using a 10 s integration time. Three spectra were obtained at a single spot to establish a baseline.

X-ray Diffraction. A single crystal of **1** was coated with Paratone oil and mounted on a MiTeGen MicroLoop. The X-ray intensity data were measured on a Bruker Kappa APEXII Duo system equipped with a graphite monochromator and a Mo K_α fine-focus sealed tube ($\lambda = 0.71073 \text{ \AA}$). The frames were integrated with the Bruker SAINT software package^[20] using a narrow-frame algorithm. Data were corrected for absorption effects using the Multi-Scan method (SADABS).^[20] The structure was solved and refined using the Bruker SHELXTL Software Package^[21] within APEX3^[20] and OLEX2.^[22] Non-hydrogen atoms were refined anisotropically. All other hydrogen atoms were placed in geometrically calculated positions with $U_{iso} = 1.2U_{equiv}$ of the parent atom ($U_{iso} = 1.5 U_{equiv}$ for methyl).

Author Information

Corresponding Authors

T. Brent Gunnoe — *Department of Chemistry, University of Virginia, Charlottesville, VA 22904, USA*; Email: tbg7h@virginia.edu

Robert J. Davis — *Department of Chemical Engineering, University of Virginia, Charlottesville, VA 22904, USA*; Email: rjd4f@virginia.edu

Authors

Zhongwen Luo — *Department of Chemistry, University of Virginia, Charlottesville, VA 22904, USA*;

Jiahua Xie — *Department of Chemical Engineering, University of Virginia, Charlottesville, VA 22904, USA*;

Nicholas Kaylor — *Department of Chemical Engineering, University of Virginia, Charlottesville, VA 22904, USA*;

Diane A. Dickie — *Department of Chemistry, University of Virginia, Charlottesville, VA 22904, USA*;

Hannah E. Ketcham — *Department of Chemistry, University of Virginia, Charlottesville, VA 22904, USA*;

Notes

The authors declare no conflict of interest.

Acknowledgment

This work was supported by the U.S. Department of Energy, Office of Basic Energy Sciences, Chemical Sciences, Geosciences, and Biosciences Division (DE-SC0000776).

We acknowledge Dr. Michal Sabat for collection of single crystal X-ray diffraction data.

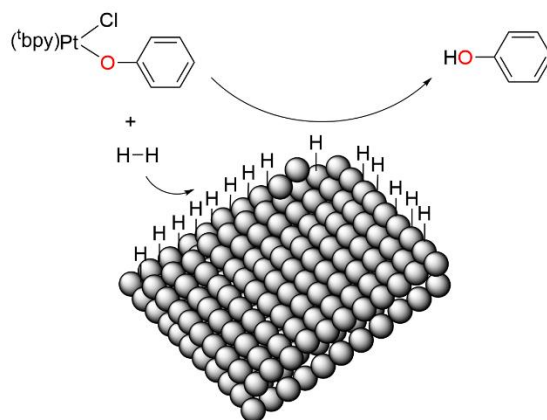
Keywords: hydrogenolysis; homogeneous; nanoparticles; heterogeneous;

References

- [1] a M. A. Stoffels, F. J. R. Klauck, T. Hamadi, F. Glorius, J. Leker, *Advanced Synthesis & Catalysis* **2020**, 362, 1258-1274; b J. H. Sinfelt, *Catal. Lett.* **1991**, 9, 159-171; c Z. Amara, M. Poliakoff, R. Duque, D. Geier, G. Franciò, C. M. Gordon, R. E. Meadows, R. Woodward, W. Leitner, *Organic Process Research & Development* **2016**, 20, 1321-1327; d D. D. Falcone, J. H. Hack, R. J. Davis, *ChemCatChem* **2016**, 8, 1074-1083; e Y. Gu, J. R. Norton, F. Salahi, V. G. Lisnyak, Z. Zhou, S. A. Snyder, *J. Am. Chem. Soc.* **2021**, 143, 9657-9663; f D. Wang, D. Astruc, *Chem. Rev.* **2015**, 115, 6621-6686; g F. Meemken, A. Baiker, *Chem. Rev.* **2017**, 117, 11522-11569.
- [2] a M. Steffan, F. Klasovsky, J. Arras, C. Roth, J. Radnik, H. Hofmeister, P. Claus, *Adv. Synth. Catal.* **2008**, 350, 1337-1348; b Y. Liu, X. Yue, C. Luo, L. Zhang, M. Lei, *Energy Environ. Mater.* **2019**, 2, 292-312.
- [3] a G. C. Bond, J. J. Garcia, *Catal. Sci. Technol.* **2017**, 7, 5294-5300; b A. Almithn, D. Hibbitts, *J. Phys. Chem. C* **2019**, 123, 5421-5432.
- [4] K. L. Sánchez-Rivera, G. W. Huber, *ACS Cent. Sci.* **2021**, 7, 17-19.
- [5] a X. Zhang, G. Cui, H. Feng, L. Chen, H. Wang, B. Wang, X. Zhang, L. Zheng, S. Hong, M. Wei, *Nat. Commun.* **2019**, 10, 5812; b T. W. Walker, A. H. Motagamwala, J. A. Dumesic, G. W. Huber, *J. Catal.* **2019**, 369, 518-525; c S. Kim, E. E. Kwon, Y. T. Kim, S. Jung, H. J. Kim, G. W. Huber, J. Lee, *Green Chem.* **2019**, 21, 3715-3743.
- [6] F. Morteo-Flores, J. Engel, A. Roldan, *Philos. Trans. R. Soc., A* **2020**, 378, 20200056.
- [7] a Z. Li, R. S. Assary, A. C. Atesin, L. A. Curtiss, T. J. Marks, *J. Am. Chem. Soc.* **2014**, 136, 104-107; b Y. Song, X. Feng, J. S. Chen, C. Brzezinski, Z. Xu, W. Lin, *J. Am. Chem. Soc.* **2020**, 142, 4872-4882; c S. Dutta, B. Saha, *ACS Catal.* **2017**, 7, 5491-5499; d A. G. Sergeev, J. D. Webb, J. F. Hartwig, *J. Am. Chem. Soc.* **2012**, 134, 20226-20229.
- [8] a Q. Meng, J. Yan, H. Liu, C. Chen, S. Li, X. Shen, J. Song, L. Zheng, B. Han, *Sci. Adv.*, 5, eaax6839; b G. R. Fulmer, R. P. Muller, R. A. Kemp, K. I. Goldberg, *J. Am. Chem. Soc.* **2009**, 131, 1346-1347; c G. R. Fulmer, A. N. Herndon, W. Kaminsky, R. A. Kemp, K. I. Goldberg, *J. Am. Chem. Soc.* **2011**, 133, 17713-17726; d J. R. Webb, C. Munro-Leighton, A. W. Pierpont, J. T. Gurkin, T. B. Gunnoe, T. R. Cundari, M. Sabat, J. L. Petersen, P. D. Boyle, *Inorg. Chem.* **2011**, 50, 4195-4211; e T. L. Lohr, W. E. Piers, M. Parvez, *Chem. Sci.* **2013**, 4, 770-775; f J. R. Webb, S. A. Burgess, T. R. Cundari, T. B. Gunnoe, *Dalton Trans.* **2013**, 42, 16646-16665.
- [9] a T. L. Lohr, W. E. Piers, M. J. Sgro, M. Parvez, *Dalton Transactions* **2014**, 43, 13858-13864; b D. H. Ess, T. B. Gunnoe, T. R. Cundari, W. A. Goddard, R. A. Periana, *Organometallics* **2010**, 29, 6801-6815.
- [10] J. R. Webb, A. W. Pierpont, C. Munro-Leighton, T. B. Gunnoe, T. R. Cundari, P. D. Boyle, *J. Am. Chem. Soc.* **2010**, 132, 4520-4521.
- [11] a Y. L. Lam, M. Boudart, *J. Catal.* **1977**, 50, 530-540; b N. Kaylor, J. Xie, Y.-S. Kim, H. N. Pham, A. K. Datye, Y.-K. Lee, R. J. Davis, *J. Catal.* **2016**, 344, 202-212; c J. Xie, B. Huang, K. Yin, H. N. Pham, R. R. Unocic, A. K. Datye, R. J. Davis, *ACS Catal.* **2016**, 6, 4206-4217; d Z. Luo, C. A. Whitcomb, N. Kaylor, Y. Zhang, S. Zhang, R. J. Davis, T. B. Gunnoe, *ChemCatChem* **2021**, 13, 260-270.
- [12] W. Zhu, Z. Luo, J. Chen, C. Liu, L. Yang, D. A. Dickie, N. Liu, S. Zhang, R. J. Davis, T. B. Gunnoe, *ACS Catal.* **2019**, 9, 7457-7475.
- [13] J. Xie, P. Duan, N. Kaylor, K. Yin, B. Huang, K. Schmidt-Rohr, R. J. Davis, *ACS Catal.* **2017**, 7, 6745-6756.
- [14] M. Boudart, D. J. Sajkowski, *Faraday Discuss.* **1991**, 92, 57-67.

- [15] F. Tao, M. E. Grass, Y. Zhang, D. R. Butcher, J. R. Renzas, Z. Liu, J. Y. Chung, B. S. Mun, M. Salmeron, G. A. Somorjai, *Science* **2008**, 322, 932.
- [16] a S. M. Klok, D. M. Heinekey, K. I. Goldberg, *Angew. Chem. Int. Ed.* **2007**, 46, 4736-4738; b B. L. Conley, S. K. Ganesh, J. M. Gonzales, W. J. Tenn, K. J. H. Young, J. Oxgaard, W. A. Goddard, R. A. Periana, *J. Am. Chem. Soc.* **2006**, 128, 9018-9019; c M. J. Pouy, E. M. Milczek, T. M. Figg, B. M. Otten, B. M. Prince, T. B. Gunnoe, T. R. Cundari, J. T. Groves, *J. Am. Chem. Soc.* **2012**, 134, 12920-12923; d G. Chen, C. Xu, X. Huang, J. Ye, L. Gu, G. Li, Z. Tang, B. Wu, H. Yang, Z. Zhao, Z. Zhou, G. Fu, N. Zheng, *Nat. Mater.* **2016**, 15, 564-569.
- [17] M. Findlater, W. H. Bernskoetter, M. Brookhart, *J. Am. Chem. Soc.* **2010**, 132, 4534-4535.
- [18] R. J. Baxter, P. Hu, *The Journal of Chemical Physics* **2002**, 116, 4379-4381.
- [19] Y.-Y. Wang, D.-J. Chen, Y. J. Tong, *ACS Catal.* **2016**, 6, 5000-5004.
- [20] Bruker (2012). Saint; SADABS; APEX3. Bruker AXS Inc., Madison, Wisconsin, USA.
- [21] G. M. Sheldrick, *Acta Cryst. A* **2015**, A71, 3-8.
- [22] O. V. Dolomanov, L. J. Bourhis, R. J. Gildea, J. A. K. Howard, H. Puschmann, *J. Appl. Cryst.* **2009**, 42, 339-341.

Table of Contents Graphic



A model reaction of noble metal-catalyzed hydrogenolysis of the Pt–OPh bond or (bpy)Pt(OPh)Cl